JOURNAL OF PROPULSION AND POWER
Vol. 13, No. 5, September–October 1997

Plug Nozzle Flowfield Analysis

T. Rommel,* G. Hagemann,* C.-A. Schley,* G. Krülle,† and D. Manski‡
DLR, German Aerospace Research Establishment, D-74239 Lampoldshausen, Germany

Results of numerical simulations of plug-nozzles are presented, and a phenomenological insight into the flowfield development at different ambient pressures is given. Therefore, a finite volume program using unstructured grids was adapted to the special boundary conditions of plug nozzles. Calculations were performed solving the Euler and Navier–Stokes equations under ideal, perfect gas assumptions. Turbulence is taken into account with a k-ε turbulence model. Numerical simulations are compared with experimental results of hot-run tests of a toroidal subscale model plug engine. Principal physical processes like expansion waves, compression shocks, and the recirculating base flow region are in good agreement with available experimental data, and can therefore be predicted well. The simulations of a full-size plug nozzle, defined for a post Ariane 5 launcher, reveal a flowfield behavior similar to the one observed with the toroidal subscale plug engine.

Nomenclature

I = impulse
M_{mix} = molar mass
p = pressure
$r_{O/F}$ = mass ratio oxidizer/fuel mixture
T = temperature
α = angle
ε = nozzle area ratio
κ = isentropic coefficient

Subscripts
a = ambient
c = combustion chamber
e = exit

Introduction

TODAY'S rocket engines, like the Ariane 5 Vulcan or SSME, apply conventional, bell-type nozzles to expand propellants burned at high pressure to low-exit pressures. First stage engines require a minimum allowable exit pressure because of nozzle flow stability limitations. Conceptual studies can be found in the literature with unconventional nozzles like plug nozzles, which provide considerable benefits in altitude adaptation of exit pressures in comparison with conventional nozzles.

Figure 1 outlines the principal design of annular plug and conventional bell nozzles. Although first conceptual studies of plug nozzles were performed in the 1950s, few experimental data are publically available on flowfield and integral performance values of real plug nozzles. However, more intensive analytical studies were done in the 1950s and 1960s in the United States, together with various experiments.[1]

Although benefits in performance were indicated in most of the available publications, plug nozzles have not yet achieved hardware flight status. This might change in the near future because a rocket engine with a linear plug nozzle is foreseen as the propulsion system for the RLV X-33 concept of the Lockheed Martin Corporation.

Results of the theoretical and experimental studies indicate that plug nozzles have significant advantages compared with conventional nozzles, concerning the structural integration of the engine into the nozzle, but also in flowfield behavior: the whole rocket base section can be used as a plug nozzle (realization of large area ratios)[1,2]; only minor performance losses caused by truncation (the truncation of a plug nozzle is defined, following Ref. 3, by the ratio of the truncated plug length l to its full length l_i, l/l_i, Fig. 1), from the ideal contour,[3,4] leading to very short nozzles; and self-adaptation of nozzle to ambient pressures, leading to rising expansion ratios and thrust values during ascent of the rocket.[5]

Major disadvantages of annular plug nozzles are the large nozzle surfaces in the combustion chamber and throat region with high heat fluxes, leading to strong cooling requirements. Furthermore, constructive problems may arise because of tiny throat gaps, since circumferential deviations of the throat gap should be minimized to ensure homogeneous, axisymmetrical thrust.[6] Alternatively, plug nozzles with chamber and primary nozzle modules were suggested to avoid the previously mentioned shortcomings. The primary nozzles may have either a circular bell-type or rectangular form.[7]

Besides the previously mentioned benefits of plug nozzles, clustered plug nozzles offer further advantages, e.g., with regard to thrust vector control, achieved through the throttling or shutdown of individual modules or the gimbaling of individual modules.

Furthermore, a single module engine failure does not lead to total loss of mission in case of a high number of individual modules. Nevertheless, additional losses are caused by the plug-cluster concepts, named gap losses, caused by the inhomogeneous flowfield with shock–shock interaction, emanating from individual module exits.[7]

To gain insight into the flowfield of plug nozzles at different ambient pressures, numerical simulations of truncated plug nozzles were performed with different physical approaches by solving the Euler and Navier–Stokes equations, respectively. Geometrical constraints are orientated at the Ariane 5 first-stage aftbody.

Plug Nozzle Flowfield Analysis

Numerical Scheme

The numerical scheme AeroShape-3D (Ref. 8) was applied to study plug nozzle flowfields because of its local grid refinement capabilities required for resolving all major flowfield

Presented as Paper 95-2784 at the AIAA/SAE/ASME/ASEE 31st Joint Propulsion Conference, San Diego, CA, July 10–12, 1995; received Aug. 30, 1995; revision received Feb. 28, 1997; accepted for publication April 16, 1997.

*Research Engineer, Space Propulsion Division. Member AIAA.
†Professor, Space Propulsion Division.
‡Research Engineer, Space Propulsion Division.

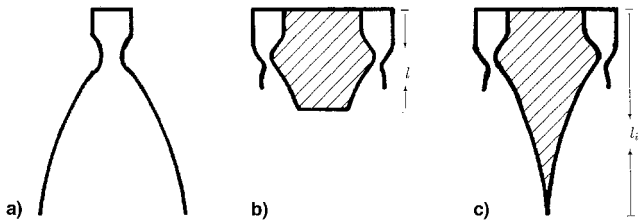

Fig. 1 Sketch of a) conventional nozzle, b) truncated, and c) annular full length (isentropic) plug nozzle.

phenomena of a plug nozzle having length scales of three different orders of magnitude. Physical modeling of that code is enhanced within the cooperation of DLR with the Moscow Aviation Institute (MAI)/Computational Aerodynamics Systems (CAS). This method was formerly used to simulate flowfield development in combustion chambers and nozzles of Russian rocket engines.

The numerical approach was developed to cope with steady as well as transient sub-, trans-, and supersonic, perfect gas flows in arbitrarily complicated geometries.[8,9] It solves the three-dimensional, transient Euler and Navier–Stokes equations, the global mass conservation, and the total energy equations. Specific heats are assumed to be constant.

The numerical method is based on an explicit finite volume approximation of the Navier–Stokes equations on a nonuniform, unstructured, rectangular mesh covering the computational domain together with an arbitrary nozzle contour. The scheme is monotonous everywhere [restriction on the total variations being of the total variation diminishing (TVD) type], and ensures the second-order-accurate approximation of the differential equations.

Solution singularities (shock waves, contact discontinuities, boundary layers, etc.), and the nozzle shape (sharp edges) are resolved by mesh refinement in their vicinity. Unrefinement is done in domains where the flow is close to the uniform one. After every computational cycle (for the transient case), or after certain residual decreases below a prescribed limit (for the steady-state case), local refinement and unrefinement according to the solution take place (flowfield adaptive grid).

Turbulence of the flowfield is taken into account using the k-ε model. Coefficients of the k-ε model are set to their standard values. Wall-damping effects on turbulent structures, and thus, anisotropic behavior of the dissipation rate, are considered by the wall function approach. Further details on the numerical method and its application to several internal and external flow problems can be found.[8,9]

Subscale Plug Nozzle Validation Test Case

In 1970, DLR performed hot run tests with plug nozzles using a toroidal rocket chamber with a chamber diameter of approximately 0.4 m (see Fig. 2 and Ref. 1). These investigations were performed with gas–oil and nitric acid. The thrust level of the toroidal rocket chamber with the plug nozzle was 15 kN at 12-bar chamber pressure. A photograph of these tests is shown in Fig. 2. For comparison of the experimental results with numerical computations, the flowfield of the toroidal plug nozzle was calculated with the numerical method presented earlier. Figure 2 shows the Mach number distribution in the combustion chamber and nozzle, both with a full gray map and isolines. Plenum chamber data of the numerical simulation result from a simulated combustion of gas–oil and nitric acid: T_c = 2980.0 K, p_c = 12.0 bar, M_{mix} = 24.566 g/mole, and κ = 1.13. The flow expands into an atmosphere, which consists of an equal gas composition with an ambient pressure of 1 bar. The numerical and experimental results are comparable concerning their principal flowfield development. However, the photograph of the experiment gives a total of the flowfield, whereas Fig. 2 shows Mach number distribution in the cross section of the centerline. Principal physical processes like expansion waves, compression shocks, Mach discs, and the recirculating base flow region are in good agreement with the photograph. Both the experiment and the numerical simulation show that the flow separates from the conical plug body before reaching its truncated end. A more detailed comparison cannot be done because of the lack of experimental data.

Recent results on experiments with plug nozzles published by Tomita et al.[10] also revealed separation of the flow from the central plug body for conical contours. In contrast, no separation was observed for contoured central plug bodies, designed with the method proposed by Angelino.[11]

Recent numerical simulations of contoured plug nozzles performed by the authors, within an European Space Agency contract on advanced rocket propulsion, also show that no flow separation occurs from contoured central plug bodies of full length. Principal flowfield developments predicted by these numerical simulations are again in good agreement with published experimental data.[10]

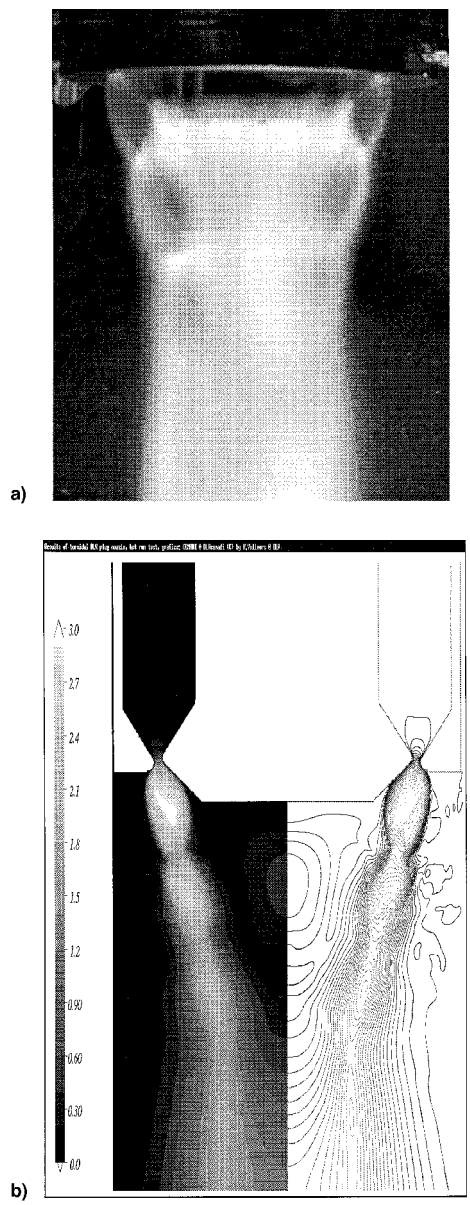

Fig. 2 Plug nozzle flowfield: Experiment vs numerical simulation: a) toroidal plug nozzle experiment with gas–oil/nitric-acid propellant combination (side view photograph) and b) computational results of toroidal plug nozzle, Mach number distribution, full gray and isolines, centerline section.

Geometry of Full-Scale Plug Nozzle

The geometry of the plug nozzle was chosen for a post-Ariane 5 launcher having the same base area as the Ariane 5 (Ref. 1), but with five Vulcan engines mounted on the aftbody. The o.d. of the plug nozzle is 4.5 m. Its nominal thrust is equivalent to the thrust of five Vulcan engines. Chamber stagnation conditions are similar to corresponding Vulcan data and are summarized: T_c = 3538.0 K, p_c = 102.0 bar, $r_{O/F}$ = 6.0, M_{mix} = 13.5 g/mole, and κ = 1.2. The geometrical area ratio of the plug nozzle, calculated as the ratio of the total area of the plug nozzle (with a diameter of 4.5 m), and its throat area is $\varepsilon \approx 55$.

For first calculations, a toroidal chamber and throat is assumed. The area ratio of the combustion chamber is 3, resulting in a throat diameter of approximately 2 cm. The contour of the combustion chamber is described by circular arcs. The divergent parts are conical, with an angle between the inner and outer contour of α = 40 deg. Figures 3 and 4 show the geometry of the plug nozzle. The area ratio of the primary nozzle exit is chosen for an expansion of the fluid to an exit pressure of 1 bar, resulting in an area ratio of $\varepsilon \approx 11.5$. This primary nozzle region is shown in Fig. 5, together with the finally adapted, finite volume mesh used for the following simulations. (Figure 4 shows the truncated plug nozzles.)

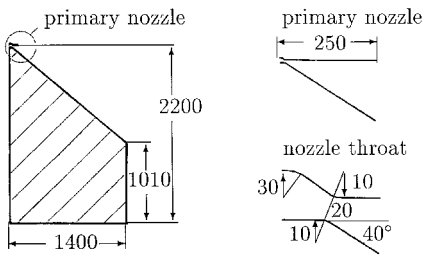

Fig. 3 Sketch of plug nozzle geometry (all lengths in millimeters).

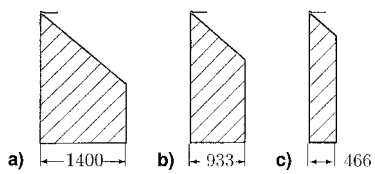

Fig. 4 Sketch of plug nozzle geometry: a) 53, b) 35, and c) 17% truncations (all lengths in millimeters).

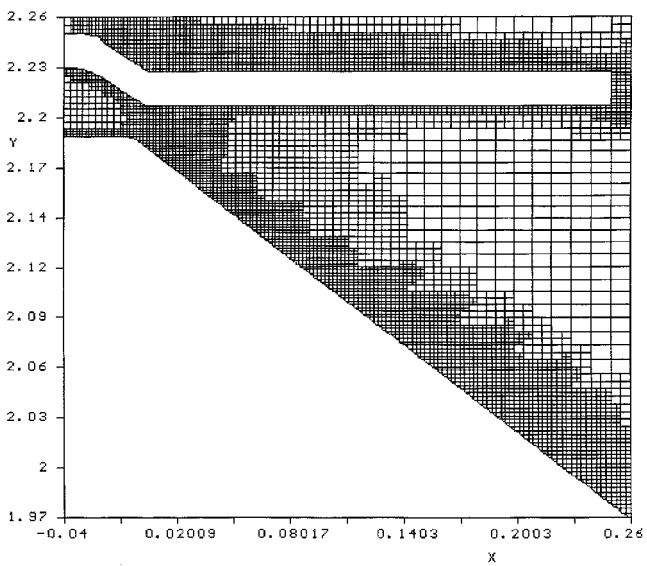

Fig. 5 Throat region with finally adapted mesh, Navier–Stokes case.

Although design methods for the central plug body based on methods of characteristics exist,[11] within this first approach in numerical simulations of plug nozzle flowfields, the geometry of the central plug body is assumed to be conical. Thus, this geometry is similar to a plug nozzle design proposed by General Electric in the late 1960s (Ref. 12).

Computational Results

In conventional bell-type nozzles, viscous effects dominate only in the vicinity of the nozzle wall. Thus, the principal flowfield development can be well predicted by solving the Euler equations for inviscid flow. To show how the flowfield of plug nozzles develops with and without consideration of viscous effects, both Euler and Navier–Stokes calculations of this plug nozzle were performed. Transient startup of the nozzle flow is simulated by a linear increase of the chamber pressure during the first thousand iterations.

Flowfields of the plug nozzle at 1-bar ambient pressure for both Euler and Navier–Stokes simulations are shown in Figs. 6 and 7, respectively. The sketch in the lower part of both Figs. 6 and 7 emphasizes the essential flow pattern of the different Euler and Navier–Stokes simulations. Both simulations were performed without any external surrounding flow; the exhaust gases expand into an ambience at rest.

The Euler simulation was performed assuming slip conditions on the walls. The flow expands through the divergent primary nozzle with its upper and lower nozzle wall. After passing the outer lip, a freestream boundary establishes at the outer side of the flowfield, which is directly influenced by the ambient pressure. Upstream of the edge of the truncated plug nozzle, which is formed with the inner wall and the base of

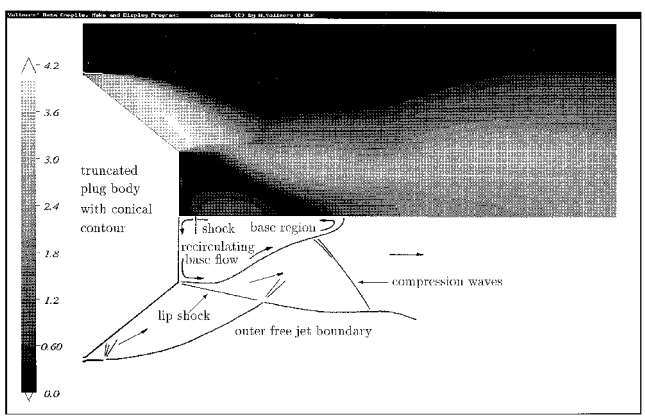

Fig. 6 Plug nozzle flowfield assuming slip-conditions on the walls, Mach number distribution, Euler case, ambient pressure p_a = 1.0 bar.

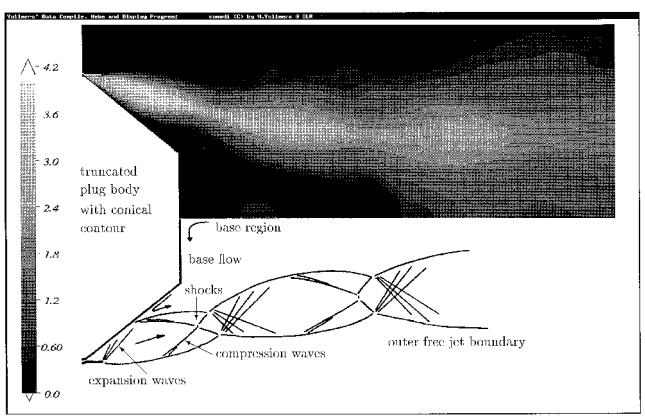

Fig. 7 Plug nozzle flowfield assuming no-slip-conditions on the walls, Mach number distribution, Navier–Stokes case, ambient pressure p_a = 1.0 bar.

the plug, the pressure in the supersonic flow regime near the wall is significantly lower than ambient pressure. In contrast, the pressure level in the base region is approximately two times higher than ambient pressure. The flow is bent around this edge, forming a separation shock (named exit lip shock), as a result of higher pressures in the wake region behind the nozzle. The flow then expands inward after separating from the truncated plug and passing the lip shock.

A sub/supersonic recirculation flow establishes in the base region, forming a closed wake form with a shock crossing the axis of symmetry in the vicinity of the base wall. This recirculation is driven by a vortex expanding into the base region during the transient startup of the nozzle flow, because there are no viscous effects forming a shear layer, which could further drive this recirculating flow. Farther downstream near the centerline, the expanding flow is turned back to axial direction, inducing recompression waves running outward through the flowfield.

The Navier–Stokes case with no-slip conditions on the wall reveals a fundamentally different flowfield development. The initial expansion process in the primary nozzle is similar to that of the Euler simulation. After emanating out of the primary nozzle exit, the flow overexpands near the wall of the central plug body like in the Euler case, but then separates from the wall because of viscous effects. The character of the flowfield downstream of the separation point is similar to that of an overexpanding plume of a conventional nozzle. In the base region, a sub- and supersonic recirculation zone develops, with a pressure level slightly higher than in the ambience. This form of the base flow is named open wake, because it is directly influenced by the ambience. Figure 8 shows the base pressure distribution at different ambient pressures. The flow structure of this Navier–Stokes simulation is comparable with experimentally obtained results of plug nozzle flowfield development (Fig. 2). It must be pointed out that the flowfield simulation of truncated plug nozzles with strong interactions of inviscid and viscous flow regimes cannot be accurately predicted by solving the inviscid Euler equations.

Various simulations of the plug nozzle flowfield at different ambient pressures have been performed, with ambient pressure values of p_a = 1.0, 0.8, 0.5, 0.1, and p_a = 0.01 bar.[6] With the latter ambient pressure value of p_a = 0.01 bar, the influence of an external flow has been studied (Fig. 9). The expansion process in the divergent primary nozzle cannot be influenced by ambient pressure, and thus is equal to the p_a = 1.0-bar case (Fig. 7). Since the exit pressure at the outer nozzle wall is approximately p_e = 1.0 bar, a significant expansion occurs for lower ambient pressures than p_a = 1.0 bar at the outer freestream boundary. A separation of the flow from the inner wall because of viscous effects can be observed down to ambient pressure values of p_a = 0.3 bar. Beyond this value, the flow expands, bounded by the inner wall down to the edge of the base.[6]

The flow development in the base region between ambient pressures of 0.5 < p_a < 1.0 bar is similar. Because of the open wake, base pressure values are similar to corresponding ambient pressures (Fig. 8).

At lower ambient pressures, a significant change in wake flow development occurs, with the wake flow turning to a closed form similar to the wake development of the Euler calculation. The pressure within the wake flow remains nearly constant (Fig. 8), and thus, is independent from further lowering of ambient pressures. Similar results on wake flow development were previously obtained in various experiments.[1,5] This change in wake flow development occurs for this plug nozzle somewhere between 0.3 < p < 0.5 bar.

Figure 9 shows the flowfield evolution near the plug body at p_a = 0.01 bar ambient pressure with simulation of an external flow. A strong interaction occurs between the exhaust gas stream of the nozzle and the surrounding flow. A shear layer is formed between the exhaust gas and external flow. However, because of the supersonic flow, the interaction does not influence the exhaust flow expansion downward of the recompression shock, induced by the bending of the shear layer slightly downstream of the primary nozzle exit. Thus, the interaction of both streams has no further influence on the nozzle performance in the case of closed wake formation at low ambient pressures.

Figure 10 shows the pressure distribution along the inner plug nozzle wall. The numerical simulation predicts a slight overexpansion of the flow near the wall of the central plug body, which finally leads to a flow separation from the wall because of viscous effects. Beyond the separation point, a recirculation zone establishes at the wall, forming a buffer zone

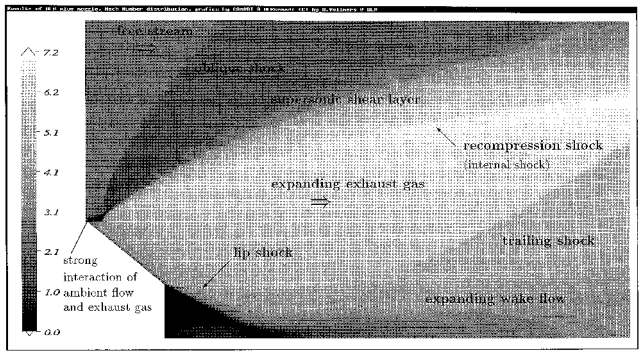

Fig. 9 Plug nozzle flowfield, Mach number distribution, Navier–Stokes case, ambient pressure p_a = 0.01 bar with external flow (with Mach number M = 2).

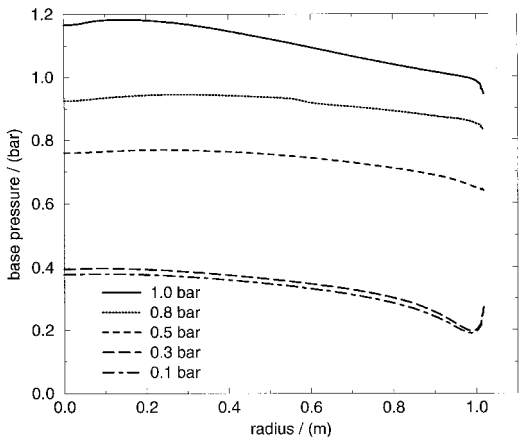

Fig. 8 Base pressure at different ambient pressures, plug with 53% truncation (radius measured from centerline).

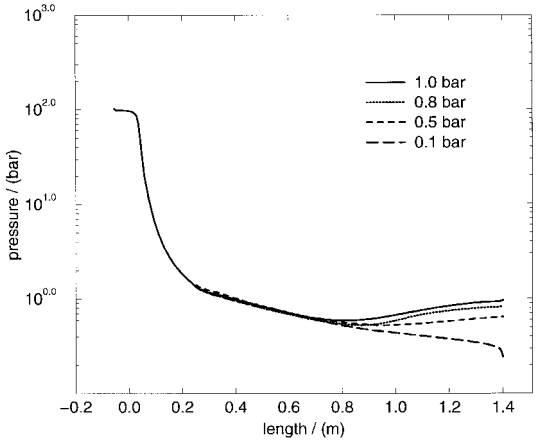

Fig. 10 Wall pressure at different ambient pressures, plug with 53% truncation (position x = 0 m in toroidal throat).

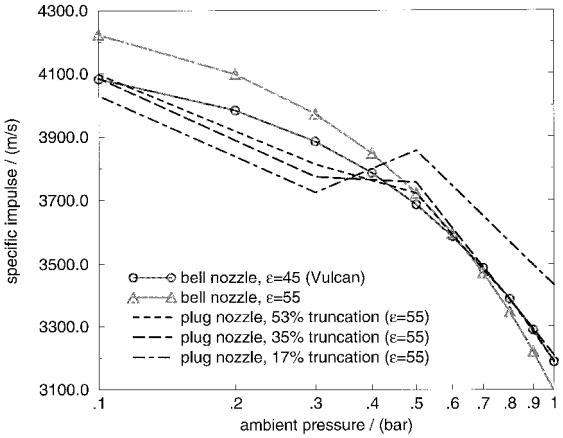

Fig. 11 Calculated specific impulses at different ambient pressures.

between the inner wall and main flow with a pressure value equal to ambient pressure. At lower ambient pressures, the separation point moves downstream toward the edge. Finally, at pressure values below $p_a = 0.3$ bar, the flow expands, conducted by the inner wall, down to the edge without separation. However, it remained questionable how correctly the separation point is predicted with the turbulence model used within these calculations.

Figure 11 shows calculated specific impulses at different ambient pressures. Data for the three plug nozzles are shown in Fig. 4, with different truncation lengths included. Furthermore, specific impulses of the Vulcan nozzle ($\varepsilon = 45$) and a bell nozzle with the same plug nozzle area ratio ($\varepsilon = 55$) are also included for comparison (performance data of both bell nozzles include performance losses of ≈0.3% caused by friction and the inhomogeneous flow in the exit plane). As previously discussed, all simulations presented in this paper were performed with ideal gas flow with constant specific heats, and thus, with a constant isentropic coefficient. Of course this simplification leads to underestimated performance data compared to real flight hardware, because the influence of high-temperature gas effects (changing gas compositions, chemistry to be in equilibrium or nonequilibrium) is neglected. But, and this is of importance, the qualitative character of these solutions with regard to the principal flowfield phenomena, and when compared with each other, is preserved.

For higher ambient pressures, $p_a > 0.4$ bar, numerical simulations of the different plug nozzles predict higher specific impulses when compared to both bell nozzles. For lower ambient pressures, however, the specific impulses of both bell nozzles are higher. Even the Vulcan nozzle with the lower exit area ratio has slightly better performance than the plug nozzles. Thus, vacuum performance of these truncated plug nozzles is significantly below the theoretical vacuum performance that corresponds to their geometrical area of $\varepsilon = 55$; whereas a substantial performance increase is obtained during sea level operation.

The plug nozzles with less truncation (shorter plug body), and thus greater base areas, perform significantly better than corresponding plug nozzles with greater lengths of the truncated plug. The main reason for this gain in performance is the negative thrust contribution induced at the plug nozzle walls, where the wall pressure is below ambient pressure because of the slight overexpansion of the flow. In case of less truncation, these areas are reduced, while the base area with a pressure level slightly higher than in the ambience is increased. The plug nozzle with 35% truncation performs almost equally to the plug nozzle with 53% truncation. The flow of both plug nozzles is similar with regard to the overexpansion and separation, because the plug length of the 35% truncation is still too long to avoid flow separation upstream of the edge. Therefore, the negative thrust contribution induced by the overexpansion remains nearly constant.

In the case of the plug nozzle with 17% truncation, the conical plug contour (Fig. 4) is further shortened. The flow reaches the edge of the plug contour without significant overexpansion, and thus the negative thrust component is considerably reduced, leading to higher thrust values and specific impulses. Specific impulses of the calculated plug nozzles show a change in slope at medium ambient pressures between $0.3 < p_a < 0.5$ bar. This drop in specific impulse is caused by the previously mentioned change in flowfield development. Here, the wake flow changes from the open structure with its characteristic influence from ambience to the closed structure, where pressure in the wake remains nearly constant. At the moment where the wake flow turns over to the closed form, the pressure level in the wake reaches a value slightly lower than in the ambience, resulting in a negative thrust contribution of the whole base area, and thus, in a drop of specific impulse.[5,6] Further lowering of ambient pressures results again in a positive thrust contribution of the base area. The point where the wake flow changes its structure was not exactly determined, but must be somewhere in the range $0.3 < p_a < 0.5$ bar for this plug nozzle.

Conclusions

Plug nozzle flowfield calculations of a toroidal plug nozzle were performed with different physical models and different ambient pressure boundary conditions. Numerical results obtained are in a good phenomenological agreement with experiments formerly performed at DLR.

Euler and Navier–Stokes simulations show a significantly different flow behavior. Viscous effects as considered in the Navier–Stokes case lead to a separation of the flow from the plug body downstream of the primary nozzle exit, depending on ambient pressure magnitude.

Furthermore, the Navier–Stokes simulations reveal a different base flow development. For higher ambient pressures, the base flow remains open, leading to a direct influence of ambient pressures in the base region. At lower ambient pressures, a significant change in base flow occurs, leading to a closed form with constant pressure level inside.

The integral performance data show superior specific impulse for truncated plug nozzles during low altitude operation, when compared to bell nozzles. However, because of the change in wake flow development, at intermediate ambient pressures, a significant drop in specific impulses can be observed.

The correct prediction of the flow separation point from the plug contour with the formerly used wall function model, and thus the correct prediction of the overall performance data, remained questionable for these numerical analyses. However, this is of importance, since the predicted difference in performance between these plug nozzles and bell nozzles is over a wide range of ambient pressures compared to former estimated numerical uncertainties of around 1–2%.

Therefore, the enhancement of the wall functions used in the turbulence model of the numerical scheme was the subject of extensive work. A new semiempirical approach has been developed, which results in an accurate prediction of separation points. Various test cases have been simulated, and a good agreement with experimental data is obtained.

References

[1]Manski, D., "Clustered Plug Nozzles for Future European Reusable Launchers," DLR-IB 643-81/7, Lampoldshausen, Germany, 1981 (in German).

[2]Stanley, D. O., Engelund, W. C., and Lepsch, R., "Propulsion System Requirements for Reusable SSTO Rocket Vehicles," AIAA Paper 92-3504, July 1992.

[3]O'Brien, C. J., "Unconventional Nozzle Tradeoff Study," Aerojet Liquid Rocket Co., NASA CR-159520, Cleveland, OH, 1979.

[4]Immich, H., and Koelle, D. E., "Plug Engine System for Future

Launch Vehicle Applications,'' International Astronautical Federation, 92-0647, Aug. 1992.

[5]Sergeant, R. J., ''An Experimental Hot Rocket Model Investigation of a Plug Cluster Nozzle Propulsion System,'' Cornell Aeronautical Lab., HM-2045-Y-5(I), Huntsville, AL, 1967.

[6]Rommel, T., ''Numerical Flowfield Analysis of Non-Conventional Rocket Nozzles,'' DLR-IB 645-95/01, Lampoldshausen, Germany, 1995 (in German).

[7]Hagemann, G., Schley, C.-A., Odintsov, E., and Sobatchkine, A., ''Nozzle Flowfield Analysis with Particular Regard to 3D-Plug Cluster Configurations,'' AIAA Paper 96-2954, July 1996.

[8]Gavriliouk, V. N., Denisov, O. P., Lipatnikov, A. N., Nakonechny, V. P., Odintsov, E. V., Sobachkin, A. A., and Sergienko, A. A., ''AeroShape-3D,'' CAS Co., Moscow Aviation Inst., Moscow, 1996.

[9]Gavriliouk, V. N., Krülle, G., and Schley, C.-A., ''Numerical Simulation of Combustion Process in Rocket Combustion Chambers with Coaxial Injection,'' AIAA Paper 94-3329, July 1994.

[10]Tomita, T., Tamura, H., and Takahashi, M., ''An Experimental Evaluation of Plug Nozzle Flow Field,'' AIAA Paper 96-2632, July 1996.

[11]Angelino, G., ''Theoretical and Experimental Investigations of the Design and Performance of a Plug Type Nozzle,'' NASA TN-12, July 1963.

[12]Schoeyer, H. F. R., *Proceedings of the ESA Plug Nozzle Workshop*, ESA-ESTEC, Noordwijk, The Netherlands, 1996.